Hindawi
Advances in OptoElectronics
Volume 2018, Article ID 8094657, 7 pages
https://doi.org/10.1155/2018/8094657

Research Article

Application of M Sequence Family Measurement Matrix in Streak Camera Imaging

Ailin Liu,[1,2] **Jinjin Zhang**,[1] **and Baoping Guo**[1]

[1]*College of Optoelectronic and Engineering, College of Information Engineering, Key Laboratory of Optoelectronic Devices and Systems of Ministry Education, Shenzhen University, Shenzhen, Guangdong 518060, China*
[2]*College of Electronic and Information, Hunan Technology and Engineering University, Yongzhuo, Hunan 425100, China*

Correspondence should be addressed to Baoping Guo; bpguo@szu.edu.cn

Received 16 October 2018; Revised 12 December 2018; Accepted 19 December 2018; Published 31 December 2018

Academic Editor: Samir K Mondal

This study investigates the reduction in the resolution of the striations from the center to the edge through analysis of the imaging principle and the static experimental test of a streak tube. To improve the edge spatial resolution of the streak, we apply the compressed sensing to the X-ray streak camera imaging system and construct the compressed sensing (CS) reconstruction model for the streak camera and we implement the CS objective function by the orthogonal matching method. The reconstruction performance of the Gauss measurement matrix, Bernoulli measurement matrix, and M series family measurement matrix are compared, and the reconstruction parameters are optimized. A comparison between the original imaging results and the reconstruction results shows that the contrast ratio of the CS reconstruction is 12.2% higher than that of the original, and the limit resolution is 5 lp/mm higher than that of the original image. Furthermore, the improvement effect far from the central area is better than that at the central area. The CS reconstruction on the M series family measurement matrix can improve the image contrast ratio on the edge of the image, and, thus, static and dynamic spatial resolutions of the image are improved.

1. Introduction

In the inertial confinement fusion (ICF) research, the characteristics of the main diagnostic object are the following: the spatial scale is small (approximately 100 μm), evolution is fast (approximately 100 ps), and the state is extreme (high temperature of approximately 108 K, high density of approximately 200 g/cm^3). The X-ray streak camera, as a scientific instrument with high spatial and temporal resolution, is the main diagnostic tool in the ICF research. The core part of the streak tube is composed of a photocathode, accelerating grid, electrostatic focusing system, deflection system, and fluorescent screen. The basic principle is to map the time information of the X-ray radiation into the spatial information of visible light on the screen. Time resolution, spatial resolution, and dynamic range are three main performance indicators of a streak camera. Academician Niu Hanben [1] proved that the accumulation of the space charge effect restricts the improvement of the spatial and temporal resolution of a streak camera. Some progress has been made in improving the spatial and temporal resolution of a streak camera. The Xi'an Institute of Optics and Precision Mechanics, Chinese Academy of Sciences [2], uses a traveling wave deflector to implement the short magnetic focusing technology, which overcomes the deceleration field in the electrostatic focusing mode. The flat electrode structure technology is adopted by the France Photonis Company [3]; this technology can reduce the dispersion time of the electron bunch. The Institute of Optics and Electronics of Shenzhen University [4] has designed a large format tube; in addition, streak tubes with various structures, such as accelerating grid and accelerating slit channel with combined plate electrodes, also exist. The above methods can improve the spatial and temporal resolutions of the streak camera.

The position of the electron beam emitted from different heights of the streak tube is not on the same plane, but on a parabola. An ordinary streak camera uses a flat screen or a spherical fluorescent screen; however, the actual surface of the electron beam is not a complete sphere. As a result, the image and the screen are not completely fitted; therefore,

defocus will occur when the nontangent position of the electron beam is projected on the screen. In actual testing, when adjusting the focus voltage to achieve the best resolution at the center of the cathode, the other off-axis electron beams are not on the optimal image plane. This behavior is similar to that of the optical mirror field curve and, thus, the central axis is the focus area, high static spatial resolution can be obtained, the off-axis area is a defocus area, and the spatial resolution is reduced.

Compressed sensing (CS) can recover from undersampled sparse data to achieve optimal real target images. When the imaging system reduces the intensity of the light source and reduces the exposure time of a charge-coupled device (CCD), the image is reconstructed by CS, and a target image similar to the original condition can be obtained. The Shenzhen advanced technology research institute of CAS applied CS to solve the defocus problem caused by the midfield curvature of acousto-optic imaging [5]; inspired by this, CS is used to improve streak camera spatial resolution.

2. Methods

2.1. Imaging System. The X-ray streak camera mainly consists of the following core parts: micro-channel plate enhancement module, high-voltage and low-voltage power supply modules, scanning circuit control module, image acquisition module (CCD), and image recording system (computer). The imaging principle is that the diagnostic information, such as time, time interval, intensity distribution, and other diagnostic information of the X-ray incident pulse are linearly transmitted to the electronic pulse by the photoelectric effect of the photocathode. Next, the electron beam is accelerated and focused by an electro-optical imaging system consisting of electrostatic focusing or magnetic focusing. After the deflection of the scanning circuit, the time information of the electron beam is projected onto the space dimension, the electro-optical conversion is conducted through the screen, and the location and intensity information are recorded through the CCD to the computer [4, 6]. The streak camera system is shown in Figure 1(a).

By combining a streak camera with 2D detectors such as a CCD, it can provide all types of ultrafast time information, spatial information, and intensity (or spectral) information; correspondingly, the main parameters are the time resolution, spatial resolution, and dynamic range [7, 8]. The time resolution and spatial resolution of the streak camera used in this study has minimum time interval and the smallest space details that a streak camera can record, respectively. The resolution is an important indicator of the streak camera.

2.2. Space Modulation Transfer Function and Spatial Resolution. For a practical electronic optical system, because of aberration, the image formed by a point passing through the system is not an ideal point. Its intensity extends outward from the center and spreads into a bright spot, which is darkened all around. The distribution of space can be represented by a point spread function (PSF) [9]. The distribution of the PSF reflects the imaging properties of the electron optical system. The electron optical system is a linear translation invariant transmission system. The electron beam before and after transmission is the object and image of the system, respectively. Csorba [10] proposed a formula to represent the spatial modulation function of the electron optical imaging system. In the formula, ρ_c is the focusing error coefficient.

$$\mathrm{MTF}(\mathrm{f}) = \exp\left[-\left(\pi\rho_c f\right)^2\right] \tag{1}$$

The contrast transfer function of the system corresponds to the square wave image. The modulation transfer function of the system corresponds to the sinusoidal image, and it can be obtained from the Fourier transform.

$$\mathrm{MTF}(\mathrm{f}) = \frac{\pi}{4} CTF\left(f\right) \tag{2}$$

2.3. Compressed Sensing. The CS method can use undersampling to recover sparse and compressed signals. Compressed observation is denoted as $y = \Phi x$, where y is the observed vector (M×1), and x is the original signal(N×1) (M≪N). x is generally not sparse; however, it is sparse in a transformation domain Ψ, such as the cosine transform, Fourier transform, and wavelet transform, which have a transformation in the form of $x = \Psi\theta$. θ in the formula is K sparsely, i.e., θ has only K nonzero terms. Here, $y = \Phi\Psi\theta$, order $A = \Phi\Psi$; thus, it follows that $y = A\theta$. In a streak camera, if the measurement data obtained from the CCD are y and the measurement matrix related to the imaging system is Φ, then $y = \Phi\theta = \Phi\Psi^{-1}x$. At this point, CS becomes a part of the X-ray scanning imaging system. The reconstruction of sparse transformation Ψ can be obtained by solving the optimization problem under the condition of bundle [11, 12].

$$\begin{aligned} \min \quad & \|x\|_1 \\ \text{s.t.} \quad & y = \Phi\psi^{-1}x \end{aligned} \tag{3}$$

To reconstruct the streak images formed in the defocus region of a streak camera, a reconstruction model based on CS is constructed [5], given as (5):

$$\arg\min F = \left\|\Phi\psi^{-1}x - y\right\| + \alpha\|x\|_1 + \beta TV\left(\psi^{-1}x\right) \tag{4}$$

Equations (3) and (4) can also be written as

$$\arg\min F = \left\|\Phi\psi^{-1}x - y\right\| + \alpha\|x\|_1 + \beta TV\left(\theta\right) \tag{5}$$

The cosine transformation is used in the formula of Ψ. In addition to the $\ell 1$ norm of the sparse domain, the total signal variation penalty term is also incorporated into the objective function to improve the accuracy of reconstruction. The first one on the right-hand side of (5) is to reconstruct the mean square error between the image and the measured value, and the second item is the $\ell 1$ norms for x; the third item TV is the signal variation penalty factor [13]. In addition, α and β are the equilibrium parameters that determine the balance between data compatibility and sparsity. Overbalance may result in reconstruction distortion, with only the proportion being close to the objective value; to achieve the

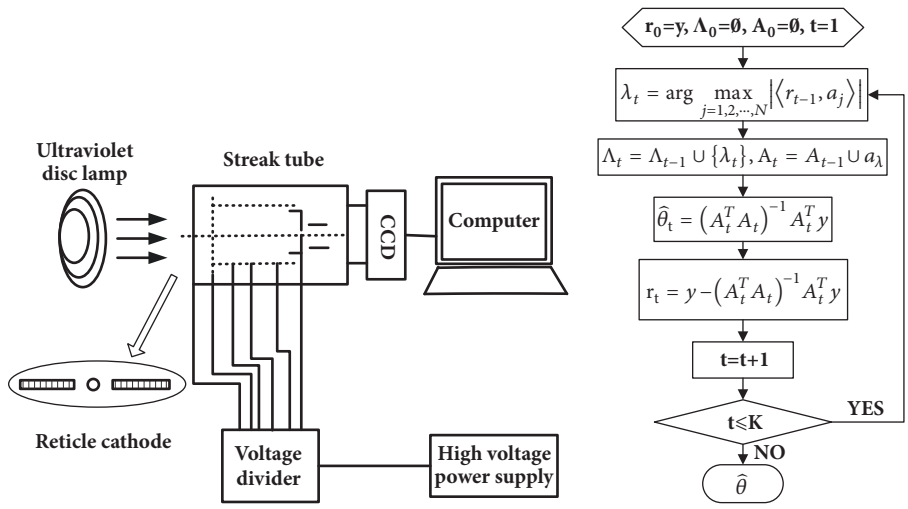

Figure 1: Schematic diagram of the experiment and the soft realization flow chart. (a) Schematic diagram of the streak camera experiment. (b) CS-OMP realization flow chart.

best reconstruction, in the experiment, the optimal balance parameter is determined from the optimal balance parameter by trying different combinations ($\alpha = 0.05$ and $\beta = 0.9$). A test schematic diagram and the software implementation process are shown in Figure 1(b).

3. Experiment

3.1. Streak Camera Static Test Subsection. The fluorescent screen (Φ52 mm) is coupled to a reduced cone (1.3:1) of light; thus, the PI2048 CCD of size 27.6 × 27.6 mm^2 cannot cover the entire cone of light on the side of full cover the fluorescent. The streak contrast value obtained from the test image is given in the first column. From 1.2 mm near the off-center axis, the fluorescent screen was sampled at intervals of 3.5 mm and values of 4.7 mm, 8.2 mm, and 11.7 mm, with contrast of 21.6%, 30.2%, 45.1%, and 48.4%, respectively; the spatial resolution is the limit resolution when the contrast transfer function CTF is 0.05. The central resolution of the image tube can be calculated using formula (1), which resulted in 31 lp/mm, edge resolution is 20 lp/mm, and the resolution of the delimit streak decreases from the center to the edge. The experimental results are consistent with the analysis results of the field curvature defocus phenomenon.

3.2. Compressed Sensing Algorithm Implementation. The objective function of CS is solved using the orthogonal matching method [14, 15]; the algorithm implementation flow diagram is shown in Figure 1(b). In the flowchart, r_t represents residual value, and t represents the number of iterations, Λ_t is an index set for the t iterations (column ordinal), λ_t represents the index found in the t iterations, a_j represents the j column of the matrix A, A_t represents a set of columns of matrix A selected by index Λ_t, θ_t is a column vector of T × 1, ∪ represents set merge, and <.> represents the vector inner product. The random Gaussian measurement matrix and the Bernoulli measurement matrix are selected for the measurement matrix, and the effects of three types of measurement matrices on the defocus problem caused by the field curvature of the streak camera are compared.

3.3. Construction of a Measurement Matrix of M Sequence Family (MSMM)

3.3.1. Trace Function. Assuming that β is the original domain element of the finite field GF (q), then all domain elements of GF (q) can be generated by the power of 0 and β, namely, 0, $\beta^0 = 1, \beta, \ldots, \beta^{q-1}$. Among them, the post q-1 nonzero elements constitute the multiplicative group GF(q)\{0}, which can also be denoted as GF (q) ∗ [16].

Definition 1. Let n be positive integers; thus, the trace function from GF (2^n) to GF (2) is

$$Tr(x) = x + x^2 + \cdots + x^{2(n-1)}, \quad x \in GF(2^n) \tag{6}$$

3.3.2. Construction of the Measurement Matrix. The measurement matrix of M sequence family is a bipolar matrix composed of +1 and −1. The size is fixed to $(2^n - 1) \times 2^{n+1}$ (n≥3), and the concrete implementation is as follows [17].

Step 1. According to the length of information $N = 2^{n+1}$ (n≥3), when n is odd, select the trace representation function shown in (6). When n is even, select the trace representation function shown in (7).

$$f_{\lambda_0,\lambda_1}(x) = Tr(\lambda_0 x) + Tr(\lambda_1 x^3) + \sum_{i=2}^{l} Tr\left(x^{1+2^i}\right), \quad x \in GF(2^n)*, \ \lambda 0, \lambda 1 \in GF(2^n) \tag{7}$$

Table 1: Comparison of the static spatial resolution of the streak camera in the experiment.

SSR (lp/mm)	DCA (mm)	OI CTF (%)	OMP- G CTF (%)	OMP- B CTF (%)	OMP-MSMM CTF (%)
22	1.2	21.6%	23.7%	24.2%	25.2%
18	4.7	30.2%	35.2%	38.1%	40.5%
12	8.2	45.1%	50.1%	54.2%	60.4%
10	11.7	48.4%	55.8%	65.8%	68.1%

SSR: streak spatial resolution; DCA: distance from the centre of the axis; OR: original image; GM: Gaussian measurement; BM: Bernoulli measurement; MSMM: M sequence family measurement matrix.

Table 2: Comparison of the limit spatial resolution of the streak camera in the experiment.

SSR (lp/mm)	DCA (mm)	LSR (lp/mm)	OMP-G LSR (lp/mm)	OMP-B LSR (lp/mm)	OMP-M LSR (lp/mm)
22	1.2	31	32	32	32
18	4.7	28	30	32	33
12	8.2	23	25	27	29
10	11.7	20	23	26	28

SSR: streak spatial resolution; DCA: distance from the center of the axis: LSR: limit spatial resolution.

$$Output = \begin{cases} 1, & Input = 0 \\ -1, & Input = 1 \end{cases} \quad (8)$$

Step 2. Select the original domain elements βon GF (2^n). Order $b_t^{\lambda 0,\lambda 1} = f_{\lambda 0,\lambda 1}(\beta^t)$; here, $t \in \{0, 1, \ldots, 2^n - 2\}$, $\lambda_0 \in$ GF(2^n). Order $b_t^{\lambda 0} = \{b_0^{\lambda 0}, b_1^{\lambda 0}, \ldots, b_{2n-2}^{\lambda 0}\}$, $b^{\lambda 0}$ is a binary sequence with a period of $2^n - 1$. When the value of λ_0 is fixed, the binary sequence, m sequence $b^{\lambda 0}$, can be obtained. The input and output transformations of the elements of λ_0 are conducted by successive passes (8), and a bipolar sequence is obtained. For iterative values of parameters λ_0 in a finite field GF(2^n), a bipolar sequence family $\{c^{\lambda 0} \mid \lambda_0 \in GF(2^n)\}$ of 2^n can be obtained. Arranging elements as column vectors can form matrices A_1. Another primitive domain element on GF (2^n) is selected, and the corresponding matrix A_2 can be obtained.

Step 3. In the two matrices obtained above, the line extension is in the form of $A = [A_1, A_2]$. Thus, the measurement matrix of this study can be obtained.

3.4. Analysis of the Experimental Results

3.4.1. One-Dimensional Signal Compression Sensing Reconstruction. To generate a sampled K sparse signal x, the support position is selected randomly, and the Gauss distribution with the support value obeys the standard; its length is 2^n+1. For each rare sparsity K, which is generated 1000 times with Matlab, the Orthogonal Matching Pursuit OMP algorithm is selected for the reconstruction algorithm; if the resulting X_R of the reconstruction is satisfied with $\|X - X_R\| < 10^{-6}$, then it is believed that the reconstruction experiment is successful and the probability of reconstruction is the ratio of exact reconstruction to the total number. Under two conditions of no noise and noise. Regarding the reconstruction performance of the measurement matrix MSMM, the Gauss random measurement matrix and the Bernoulli random measurement matrix are compared. For order n = 8, after generating a measurement matrix with a size of 255 ×512, sparsity k = 1-85. The comparison curves of the reconstruction probability under different sparsities are shown in Figure 2(a). For the sampled signal with a signal-to-noise ratio of 30 dB, comparison curves of the reconstruction probability under different sparsities are shown in Figure 2(b). According to graphs (a) and (b), in a noisy environment and a no-noise environment, the signal recovery effect of the matrix MSMM is better than that of the Gaussian matrix and the Bernoulli matrix of the same size.

3.4.2. Image Reconstruction of the Streak Camera. In the observable cathode range, the background noise of the image should be deducted in practical application. The formula for calculating the contrast in actual calculation is as follows [18]:

$$C = \frac{(I_{\max} - I_{nos}) - (I_{\min} - I_{nos})}{(I_{\max} - I_{nos}) + (I_{\min} - I_{nos})} = \frac{I_{\max} - I_{\min}}{I_{\max} + I_{\min} - 2I_{nos}} \quad (9)$$

In the formula, Imax, Imin, and Inos are the intensity values of the streak, intensity of the adjacent dark lines, and background noise of the images, respectively. The contrast between the three matrix reconstruction diagrams and the original diagram is given in Table 1. The limit static spatial resolution is calculated from the spherical fluorescent screen, and the corresponding limit resolution is obtained as shown in Table 2. The following results are obtained: (1) the image restoration effect of the MSMM matrix is better than that of the Gaussian matrix and the Bernoulli matrix of the same

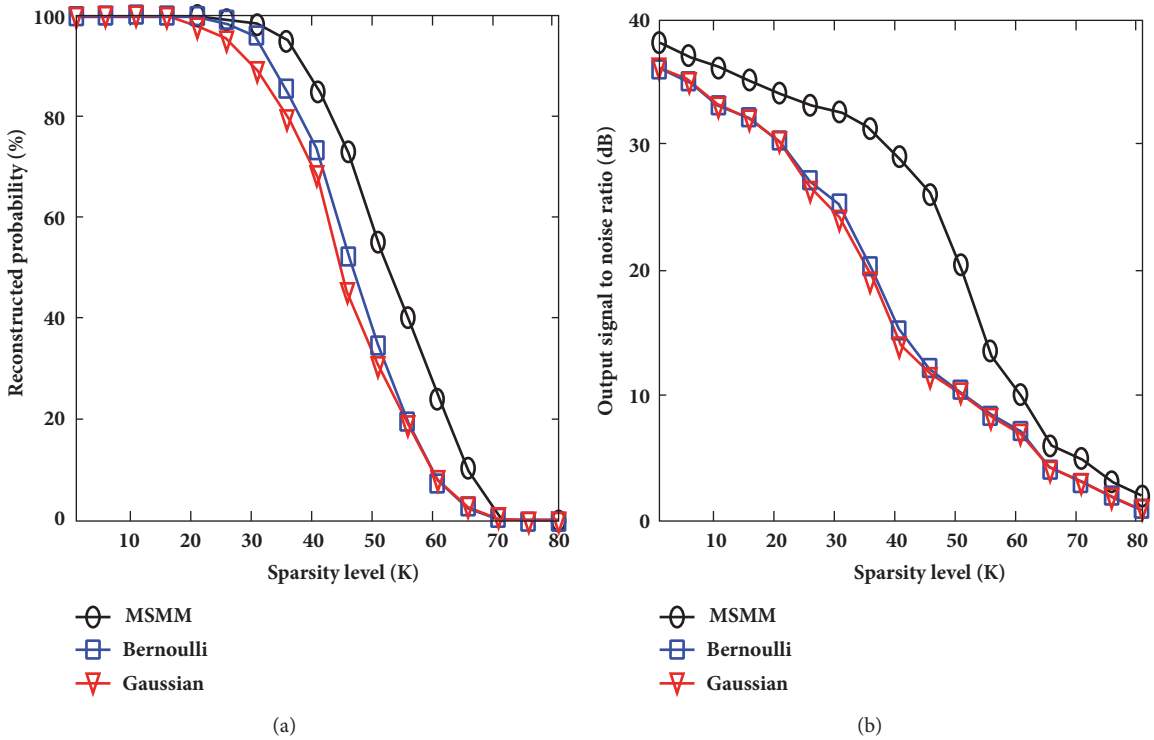

Figure 2: Comparison of the effect of measurement matrix reconstruction. (a) Reconstruction probability under different degrees of sparsity. (b) Output signal-to-noise ratio under different degrees of sparsity.

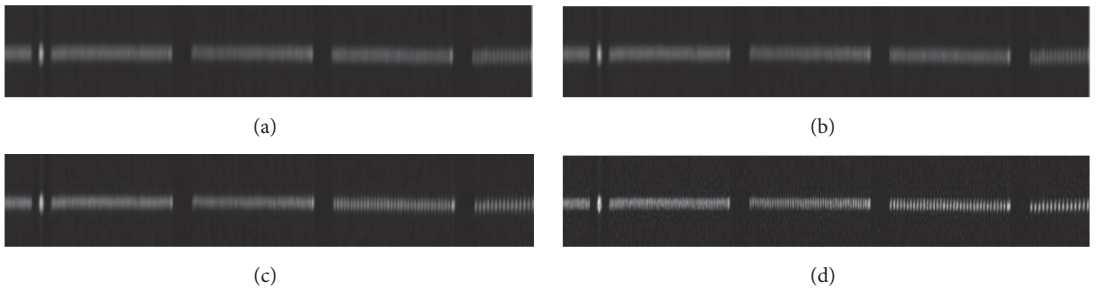

Figure 3: Comparison of the effect of measurement matrix reconstruction. (a) The original image; (b) reconstruction on the Gaussian matrix; (c) reconstruction on the Bernoulli matrix; (d) reconstruction on the MSMM.

size from Table 1. (2) The contrast of the MSMM matrix reconstructed image is 12.2% higher than that of the original image. (3) The average limit resolution is increased by 5 lp/mm. (4) The distance from the axis center is 1.2 mm, the contrast is increased by 3.6%, and the limit resolution is increased by 1 lp/mm. (5) At a distance from the axis center of 11.7 mm, the contrast increased by 19.7%; and the limit resolution increased by 8 lp/mm. As a result, the edge contrast of the image is increased more obviously than that of the central area; the ultrafast static image is shown in Figure 3 and the central line intensity in Figure 4 is shown in the ultrafast static image, with the improvement of contrast in the edge area being more obvious than that in the central area. Finally, the experiment is carried out in the dynamic imaging process of the streak camera, the dynamic streak image is shown in Figure 5(a). The longitudinal coordinates indicate scanning direction (time-resolved channel), and the abscissa indicates the direction of the slit. After completing the experiment of CS reconstruction, a single time-resolved channel is randomly selected for comparison in the reconstructed dynamic streak image, the intensity image of a single time-resolved channel is shown in Figure 5(b), and the proposed method has obvious effect on improving strength of the dynamic streak image.

4. Conclusion

The position of an electron beam emitting at different heights on the streak cathode is not on the same plane, but is on

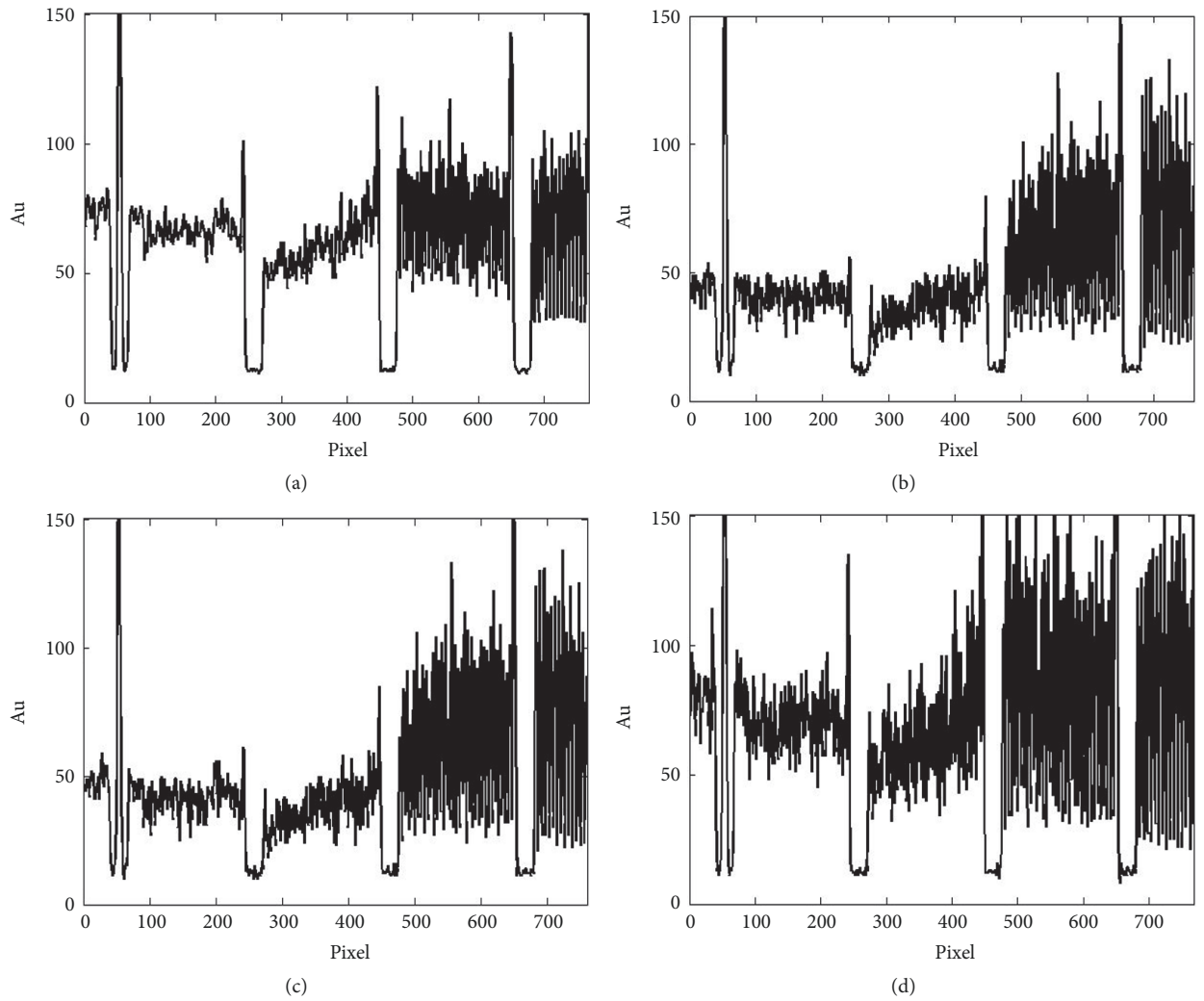

Figure 4: Comparison of the central line strength graphs in the streak camera static image. (a) Central line strength of original image; (b) central line strength of reconstruction on Gaussian matrix; (c) central line strength of reconstruction Bernoulli matrix; (d) central line strength of reconstruction on the MSMM.

a parabola. Through analysis of the static spatial resolution test data of the streak image tube, the off-center axis area is the defocus area, and the CS algorithm is applied to improve the imaging quality of the defocus region of the streak tube camera. To achieve the best image restoration effect of a streak tube camera, a reconstruction model based on CS was constructed. The optimization of the reconfiguration parameters can be achieved by examining different combinations of equilibrium parameters. The experimental results showed the following: the static image contrast increased by 12.2%, and the limit resolution of the static test image increased by 5 lp/mm on average. At a distance of 1.2 mm from the center to the center of the axis, the contrast increase is 3.6%, limit resolution is increased by 1 lp/mm, contrast is raised by 19.7% at the center distance of the off-axis, and the limit resolution is improved by 8 lp/mm. This result showed that the contrast improvement of the edge is more obvious and the M sequence family measurement matrix compression sensing method has a certain compensation effect on the edge defocus caused by the field curve, thereby providing a new approach for improving the spatial resolution of the streak tube camera.

Data Availability

The data used to support the findings of this study are available from the corresponding author upon request.

Conflicts of Interest

The authors declare no conflicts of interest.

Acknowledgments

This research was funded by National Natural Science Foundation, Grant no. 11805137, the Shenzhen City Science

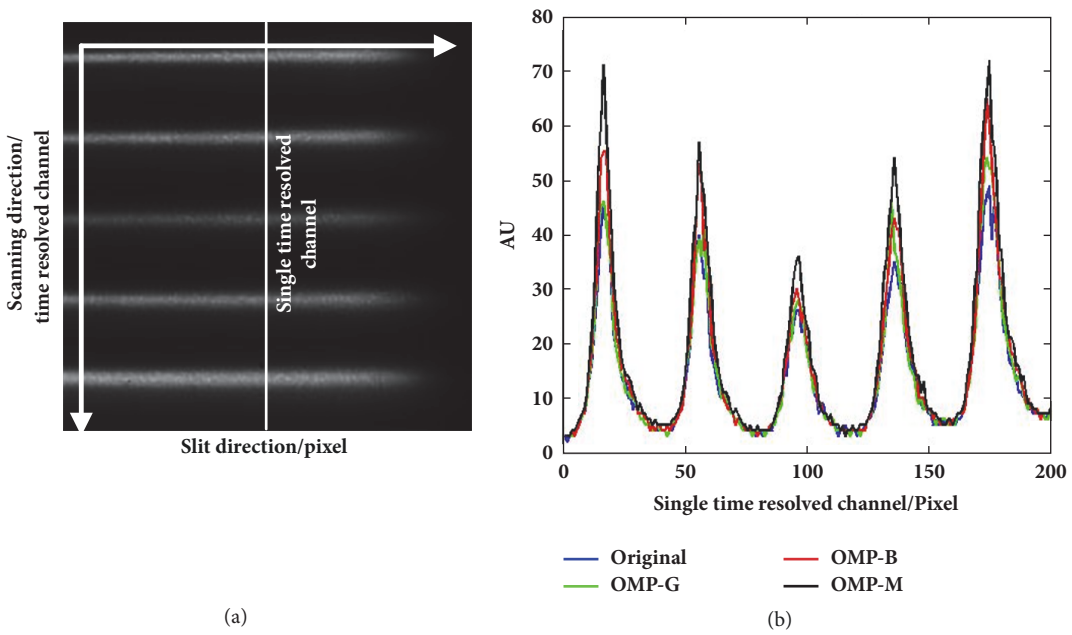

FIGURE 5: Comparison of time resolved channel in the streak camera dynamic image. (a) Streak camera dynamic image. (b) The line strength graph of single time resolved channel after reconstructed and original image.

Research Fund, Grants no. JCYJ20170818141616714 and no. JCYJ20170818102618203, and the Construct Program of the Key Discipline in Hunan University of Science and Engineering, Grant no. CS201801.

References

[1] H. Niu and W. Sibbett, "Theoretical analysis of space-charge effects in photochron streak cameras," *Review of Scientific Instruments*, vol. 52, no. 12, pp. 1830–1836, 1981.

[2] R. Liu, J. S. Tian, R. C. Miao et al., "Dynamic Characteristic Analysis on Streak Image Tube with High Temporal Resolution," *Acta Photonica Sinica*, vol. 45, no. 10, pp. 109–115, 2016.

[3] D. Schimann, A. Mens, R. Sauneuf et al., "Performance of the ultrafast streak camera C850X," *SPIE*, vol. 1757, pp. 8–18, 1992.

[4] G. Li, Z. Fang-Ke, L. Xing et al., "Development of X-ray streak camera with large dynamic range and high temporal spatial resolution," *Acta Optic Sinica*, vol. 37, no. 12, pp. 1–7, 2017.

[5] J. Meng, C. Liu, J. Zheng, R. Lin, and L. Song, "Compressed sensing based virtual-detector photoacoustic microscopy in vivo," *Journal of Biomedical Optics*, vol. 19, no. 3, Article ID 036003, 2014.

[6] I. Gorgisyan, R. Ischebeck, C. Erny et al., "THz streak camera method for synchronous arrival time measurement of two-color hard X-ray FEL pulses," *Optics Express*, vol. 25, no. 3, pp. 2080–2091, 2017.

[7] Y. Fang, X. Xu, J. Tian, and C. Pei, "Design of a control system with high stability for a streak camera using isolated ADC," *Nuclear Science and Techniques*, vol. 29, no. 2, p. 22, 2018.

[8] J. R. Howorth, J. S. Milnes, Y. Fisher et al., "The development of a streak tube with improved time and spatial resolution," in *Proceedings of the Selected Papers from the 31st International Congress on High-Speed Imaging and Photonics*, International Society for Optics and Photonics, 10328: 103280Q, 2017.

[9] Z. Yuan, T. Chen, Z. Yang et al., "Method to measure the temporal resolution of x-ray framing camera," *Optical Engineering*, vol. 57, no. 07, pp. 074101–1–074101–5, 2018.

[10] I. P. Csorba, "Modulation transfer function of image tube lenses," *Applied Optics*, vol. 16, no. 10, pp. 2647–2650, 1977.

[11] M. Lustig, D. Donoho, and J. M. Pauly, "Sparse MRI: the application of compressed sensing for rapid MR imaging," *Magnetic Resonance in Medicine*, vol. 58, no. 6, pp. 1182–1195, 2007.

[12] J. A. Tropp and A. C. Gilbert, "Signal recovery from random measurements via orthogonal matching pursuit," *IEEE Transactions on Information Theory*, vol. 53, no. 12, pp. 4655–4666, 2007.

[13] J. Wang, S. Kwon, and B. Shim, "Generalized orthogonal matching pursuit," *IEEE Transactions on Signal Processing*, vol. 60, no. 12, pp. 6202–6216, 2012.

[14] W. Jin, Z. Liu, and G. Li, "Block-based compressed sensing for neutron radiation image using WDFB," *Advances in OptoElectronics*, pp. 1–5, 2015.

[15] L. Gao, J. Liang, C. Li, and L. V. Wang, "Single-shot compressed ultrafast photography at one hundred billion frames per second," *Nature*, vol. 516, no. 729, pp. 74–77, 2014.

[16] N. Y. Yu and G. Gong, "A new binary sequence family with low correlation and large size," *Institute of Electrical and Electronics Engineers Transactions on Information Theory*, vol. 52, no. 4, pp. 1624–1636, 2006.

[17] L. Cunbo, X. Song, and Q. Lei, "Construction of compressed sensing measurement matrix based on binary sequence family," *Journal of Electronics and Information Technology*, vol. 38, no. 7, pp. 1682–1688, 2016.

[18] Z. Liwei, *Electron optics with wide beam focusing*, Beijing Institute of Technology Press, Beijing, China, pp. 345–351, 1993.